RSC Advances

ROYAL SOCIETY OF CHEMISTRY

www.rsc.org/advances

The Photocatalytic Activity and degradation Mechanism of methylene blue over Copper(II) Tetra (4-carboxyphenyl) porphyrin Sensitized TiO_2 under Visible Light irradiation

Huigang Wang,[*a,b,c] Dongmei Zhou,[a] Shaosong Shen,[a] Junmin Wan,[a] Xuming Zheng,[*a] Lihong Yu,[b] David Lee Phillips[b]

Received (in XXX, XXX) Xth XXXXXXXXX 20XX
DOI: **/b000000x

[a]*Department of Chemistry and Engineering Research Center for Eco-dyeing and Finishing of Textiles, MOE, Zhejiang Sci-Tech University, Hangzhou 310018, China*
[b]Department of Chemistry, The University of Hong Kong, Pokfulam Road, Hong Kong S.A.R., China
[c]*Department of Physics, University of Osnabrueck, 49069 Osnabrueck, Germany*

CORRESPONDING AUTHOR FOOTNOTE

Professor Ph.D. Huigang Wang

Email: zdwhg@163.com, huigwang@uni-osnabrueck.de

Department of Chemistry Phone: 00186-571-8684-3627

Zhejiang Sci-Tech University FAX: 00186-571-8684-3627

Hangzhou, 310018

China

Abstract: Copper(II) Meso-tetra(4-carboxyphenyl)porphine (CuTCPP) sensitized nano TiO_2 particles, denoted as CuTCPP-TiO_2, were synthesized to modify the photoresponse properties of TiO_2 particles. Femtosecond and nanosecond spectroscopic studies of CuTCPP and CuTCPP-TiO_2 are reported, combining both the time-correlated single-photon counting (TCSPC) technique and transient absorption measurements. The purpose is to investigate the TiO_2 photodegradation mechanism and the relationship with the initial electronic and vibrational relaxation of the S1 and S2 excited states of the sensitizer. Excitation of the Soret band, leads to multiple electronic and vibrational relaxation time scales of S2 and S1 populations, from hundreds of femtoseconds to tens of nanoseconds. The systematic and detailed studies reported here reveal that the Soret fluorescence band decays with a lifetime of 98~120 ps for CuTCPP whereas 123-398ps for CuTCPP-TiO_2, with the lifetime prolonged, the fluorescence intensity however, are greatly reduced. In addition, the S1 fluorescence was totally quenched after CuTCPP sensitized on the TiO_2. The overall picture of electronic relaxation dynamics is depicted according to these observations. The photo degradation of methylene blue (MB) over CuTCPP-TiO_2 was systematically investigated. The presence of CuTCPP molecules in the TiO_2 surface led to enhancement in its photodegradation of MB under visible light irradiation. The photocatalytic degradation kinetics of MB fitted well with Langmuir–Hinshelwood mode. Moreover the detailed short-time dynamics for visible-light induced catalytic mechanism was discussed.

Keywords: CuTCPP-TiO_2, visible-light photocatalytic, time-correlated single-photon counting, relaxation dynamics, time resolved transient absorption

1 Introduction

Most of the developed and developing industrialized nations are faced with a tremendous set of environmental problems related to the remediation of hazardous wastes and the contaminated groundwaters[1-3]. The industry waste materials are very complex, presently the physical techniques are key treatment method including adsorption[4-6], sedimentation[7], filtration[8] as well as flocculation[7]. Although these methods can transfer the pollutants from aqueous solution to solid phase, the total quantity or hazardous potential of the pollutants are recalcitrant in nature. To destroy organic pollutants in water one of the most important processes is heterogeneous photocatalysis via semiconductor[9, 10]. The vital draw-back of TiO_2 or ZnO semiconductors is that they absorb only the ultraviolet radiation whose wavelength is less than 387 nm ($\lambda \leqq 385$ nm) , which only occupy less than 5% of whole sunlight[11, 12]. Dye sensitization is considered to be a viable alternative method to modify the photoresponse properties[11, 13-15].Over the last 30 years the scientific and engineering interest in the application of dye sensitized semiconductor photocatalysis has grown exponentially[13-15].

Porphyrins are recognized to be the most promising sensitizers. In particular, metal porphyrin have been shown to be efficient photosensitizers and catalysts for a variety of oxidation reactions[16-20]. Recently, the photocatalytic activity of TiO_2 powders impregnated with Cu porphyrins has been investigated and shown to be the best one on the decomposition of 4-nitrophenol (4-NP)[18, 20].

In addition to the extraordinary experimental achievements, some mechanistic aspects and time resolved techniques have been applied to investigate on the catalytic mechanism and electronic transfer dynamics[17]. Spectroscopic investigations shown that the relaxation dynamics of

porphyrins is significantly modulated by the central metal ion in metalloporphyrins and the substitution in the macrocycle[21-23] . On the basis of laser flash photolysis measurements general mechanism as well as the corresponding primary reaction rate for heterogeneous photocatalysis on TiO_2 have been proposed[24]. Griffith etc investigated systematically the influence of porphyrin molecule structure on efficiency determining electron transfer kinetics and solar cells performance. But the research was limited in free-base and zinc porphyrin dyes[17].

After metal ions quantitively coordinate in the central cavity, the Molar extinction Coefficient of porphyrin will be strongly enhanced and the photoresponse in the visible light region is extended as well. Cu(II) porphyrins (CuTCPP) are usually four coordinated with ligands and stable against the acid-induced demetallation. With the partially filled d orbitals, Cu(II) ions are capable of fluorescence quenching by electron or energy transfer[25, 26]. Furthermore, Cu(II), with its d^9 valence electron configuration, is paramagnetic, which has be shown to increase the quenching efficiency of the metal ion[25, 26]. Therefore, the excited state of Cu(II) porphyrin (CuTCPP*) has a high possibility for electrons to inject to the conduct band of TiO_2, which is exactly different to the behavior of well-known zinc(II) porphyrins.

Moreover, Cu(II) porphyrin belong to the different group of zinc(II) porphyrins in Metalloporphyrins based on their Spectroscopic properties[27]. *Regular* metalloporphyrins contain closed-shell metal ions (d^0 or d^{10})—for example Zn^{2+} , in which the $d\pi$ metal-based orbitals are relatively low in energy. These have very little effect on the porphyrin π to π^* energy gap in porphyrin electronic spectra. *Hypsoporphyrins* are metalloporphyrins in which the metals are of d^m , m = 6–9, having filled $d\ \pi$ orbitals—for example Cu^{2+}. In hypsoporphyrins there is significant metal $d\ \pi$ to porphyrin π^* orbital interaction (metal to ligand π- backbonding) [27]. This results in very different photoexcited electronic reactions.

Based on our previously reported works on the Soret(Bx and By-band) electronic transitions and the corresponding photo relaxation dynamics of tetra (4-carboxyphenyl) porphyrin (TCPP)[28, 29], and the work on degradation mechanism of methyl orange under photo-catalysis of TiO_2[30], in this work, Copper(II) Meso-tetra(4-carboxyphenyl)porphine sensitized TiO_2 (CuTCPP-TiO_2) were synthesized and their properties of photo-generated reactive species, holes and electrons were studied by transient absorption spectroscopies and time-correlated single-photon counting (TCSPC) technique. Photocatalysis of methylene blue (MB) over CuTCPP-TiO_2 were systematically investigated.

2. Experimental Methods

2.1. Materials.

meso-tetra (4-carboxyphenyl) porphyrin were purchased from J&KCHEMICA with no further purification. TiO_2 nanoparticles (P25, d=21 nm) were purchased from Beijing Entrepreneur Science & Trading Co. DMF and MB was of analytical reagent grade quality and was used without further purification. Other chemicals were commercial products of analytical grade or reagent-grade. All the solutions were prepared with distilled water.

2.2. Synthesis

A 27.0 mg (0.15 mmol) of $CuCl_2$ were added to 42.4 mg (0.05 mmol) of the TCPP dissolved in 100 mL of DMF. The mixture was heated to reflux for 8 h and monitored by TLC until the complete disappearance of the starting material TCPP. The unreacted solid salt was filtered off and the solvent was removed under vacuum. The crude product was washed with water and then

purified by chromatography on a silica gel column with CH_3OH:$CHCl_3$=1:3 as eluant. The product CuTCPP was recovered in nearly quantitative yield. ^{1}H NMR(CDCl3, 400 MHz): δ, ppm 8.9 (s, 8H), 8.4 (d, 8H), 8.3 (s, 8H).. UV–vis (CHCl3): λmax, nm, 418 (Soret band), 540 (Q bands).

The TiO_2 sensitized by CuTCPP were obtained as follows:1g TiO_2 was added into the 100mL 0.5mmol/L DMF solution of CuTCPP. The mixture was refluxed for 5 h in dark, and then filtration to get the solids, washed with 10mL DMF 5 times and then washed with distilled water 5 times, the solids were dry, in this way, TiO_2 coupled by CuTCPP were prepared, and denoted as CuTCPP- TiO_2

2.3. Characterization

Transient Fluorescence Decay measurements were performed by using the Time Correlated Single-Photon Counting (TCSPC) technique with a confocal fluorescence microscope system (HORIBA, Ltd.). The excitation light source was a mode-locked Ar+ ion laser centered at 370 nm, operated at a frequency of 8 MHz. The fluorescence photon was collected between 540 nm and 580 nm and no counts of fluorescence from the TiO_2 or quartz substrate was detected. The femtosecond TA experiment was carried out by a femtosecond Ti:Sapphire regenerative amplified Ti:Sapphire laser system (Spectra Physics, Spitfire-Pro) and an automated data acquisition system (Ultrafast Systems, Helios). The pump laser was of 267 nm (the third harmonic of the fundamental 800 nm from the regenerative amplifier). The probe pulse was white-light continuum (450–800 nm) generated by a sapphire plate using approximately 5% of the original output from the Spitfire. Before passing through the sample the probe pulse was split into two beams: one beam travels through the sample, and the other is sent directly to a reference spectrometer that monitors the fluctuation of the probe beam intensity. The instrument response function is evaluated to be 150 fs. The nanosecond TA experiment was carried out using a LP920 laser flash spectrometer manufactured by Edinburgh Instruments Ltd. The probe light source was a 450 W ozone free Xe arc lamp producing a continuous spectrum between 150 and 2600 nm. The pump light was generated by a Q-switched Nd:YAG laser (Model: Lab 150-10 4056L; 3rd harmonic line at l = 355 nm). The TA signal was recorded with a TDS 3012C digital signal analyzer. The TA signals of all samples in the nanosecond TA experiment with the occurrence of the photocatalytic reactions were reproducible, and therefore the accumulation of photo-catalytic products was negligible.

The timedependent TA signals at different pump and probe wavelengths were fit to a multiexponential function, convoluted with a Gaussian instrument response function of 120 fs fwhm. The multiexponential function, $f(t)$)= $\sum_i Ai \exp(-t/\tau i)$ commonly used in TA data analysis, was derived on the assumption of first order reaction kinetics with parallel pathways from the first excited state.

The degradation rates of MB solutions were periodically scanned by a UV-2501 spectrophotometer (Shimadzu, Japan), and the maximum absorption wavelength of MB solution was identified at 665 nm. UV-vis spectra data were recorded in the range from 200 to 800 nm. The X-ray diffraction (XRD) patterns were recorded on D5000 Diffraction system. XPS measurements were performed with Perkin Elmer PHI 5900 and equipped with nonmonochromatizedsource (operating at 150 W).

2.4. Photocatalytic activity measurements

The photocatalytic activity of CuTCPP-TiO_2 samples was evaluated by the degradation rate of

methylene blue under visible-light irradiation. The experimental set up placed in a black box consisted of a 200 mL beaker irradiated by a 250 W, 220 V Iodine-Tungsten lamp. The distance between the lamp and the solution is 50 cm. A 420 nm cutoff filter (Schott Glass) was placed between the lamp and the beaker in order to absorb the UV light. The temperature inside the reactor was maintained at ca. 298 K by means of a continuous circulation of water surrounding the reactor.

100 mL Methylene blue（MB）aqueous solution (0.9mg/L) was mixed with 20.0 mg photocatalyst powder in the above 200 mL beaker. The mixture was stirred with a magnetic bar and bubbled with oxygen. Keep the mixture 50 min in darkness before switching on the lamp to allow the physical adsorption reach equilibrium. The initial pH value of the suspension was 4.0 and it was measured and keeps in a narrow range during the photocatalytic experiments.

The photoreactivity runs lasted 400 min. Samples of 3 mL were withdrawn from the suspension every 50 min during the irradiation. The photocatalysts were separated from the solution by centrifugation and the quantitative determination of Methylene blue was performed by measuring its absorption at 664 nm with a Shimadzu UV-2501 PC spectrophotometer. For comparison, the MB photodegradation experiment was conducted under the same conditions using Degussa P25 powder as photocatalysts.

3. Results

Understanding the dynamic processes observed in the time resolved spectra preliminary requires a deep insight into the static spectroscopic properties of the sample. Here we presented the absorption and fluorescence spectra of CuTCPP in tetrahydrofuran (THF) in Figure 1，the fluorescence spectra of CuTCPP-TiO_2 is also included. Figure 1 shows that, the Soret band and the Q band. The strongest absorption Soret band at 417.6 nm is assigned as B (0,0), where the numbers in parentheses indicate the number of quanta of the dominant Franck-Condon active vibrational mode in the upper and lower electronic states of the transition, respectively. The Q band is at 540.4 nm and assigned as Q(0,0). The lowest triplet state, T1, lies below the Q(0,0) state.

The CuTCPP and CuTCPP-TiO_2 fluorescence spectra in Figure 1 for 365 nm excitation clearly show S2→S0 fluorescence. Peaks in S1→S0 fluorescence of CuTCPP are measured at 651.5nm for Q(0,0) and 711.5 nm for Q(0,1). Correspondingly the S1→S0 fluorescence of CuTCPP-TiO_2, however disappeared, the emission intensity of Q(0,0) were quenched by TiO_2. The peak in S2 fluorescence of CuTCPP is measured at 487.7nm, whereas of CuTCPP-TiO_2 is measured at 469.0nm, blue-shifted 18.7nm after anchored to TiO_2, and the intensity is weakened. The interaction of the carboxylate group with surface Ti ions is likely to lead to the formation of Ti-O-C=O bonds. The carboxylate serves, therefore, as an interlocking group enhancing electronic coupling between the π orbitals of the phenyl and the Ti(3d) orbital manifold of the semiconductor. This coupling is rendered efficient by the presence of π electrons in the bridging group leading to increased delocalization of the π level of the phenyl and pyrrole ligand. The energy of the π level is decreased by this delocalization, thus increased the energy gap between S0 and S2 state, which explains the observed blue shift in the fluorescence spectrum.

The only pathway for electrons in S1 excited state in CuTCPP comes out to be 3 possible relaxations pathways after CuTCPP anchored to TiO_2-transferred to the TiO_2 conduction band, transferred to the triplet state or transferred to S0 state, and consequently quenched the emission

intensity of fluorescence S1 →S0 process.

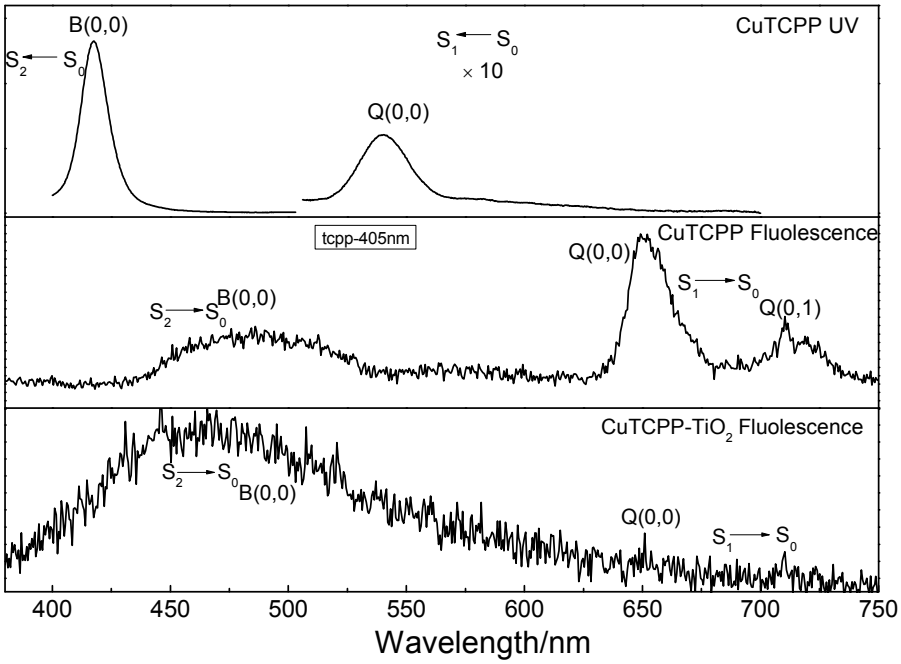

Figure 1. The UV-VIS absorption and static fluorescence spectra of CuTCPP in tetrahydrofuran solution and the fluorescence spectra of CuTCPP-TiO_2 in solid. For the fluorescence spectrum, the excitation wavelength was 365 nm, the sample concentration was 1 μM in a 5 mm cell, reabsorption may be significant below 430 nm.

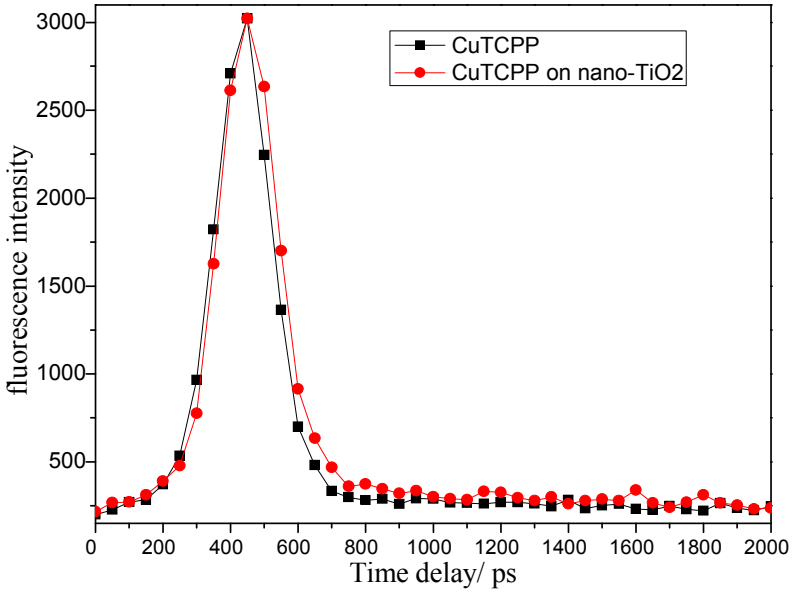

Figure 2 The normalization of the fluorescence decay profiles of CuTCPP and CuTCPP-TiO_2 (multiplied by 1.54) obtained by TCSPC.

Fig. 2 shows the fluorescence decay profiles of CuTCPP (solid) and CuTCPP-TiO_2 (solid)

respectively. The fluorescence intensity of CuTCPP-TiO_2 have been multiplied by a factor of 1.54, this means that in our experiment, the 440nm fluorescence of CuTCPP is a bit quenched by TiO_2 after UV excitation (370nm), and its lifetime becomes longer as shown in Fig. 2 (fitted with exponential function to get the lifetime of 98.2ps for CuTCPP and 123.1ps for CuTCPP-TiO_2). In a typical electron transfer process from a dye (for example N719) to anatase TiO_2 under UV excitation, the fluorescence intensity of the dye is usually quenched meanwhile with its lifetime shortened to some extent[31]. The longer life time keeps the electron-hole separation longer enough to take place the following photochemical reactions.

It is well known that the recombination of photo-generated electrons and holes in nano-sized TiO_2 occurs in several microseconds under vacuum conditions. We also characterized the CuTCPP-TiO_2 with Transient absorption spectroscopy in the femto and nanoseconds to study the recombination processes of electrons and holes.

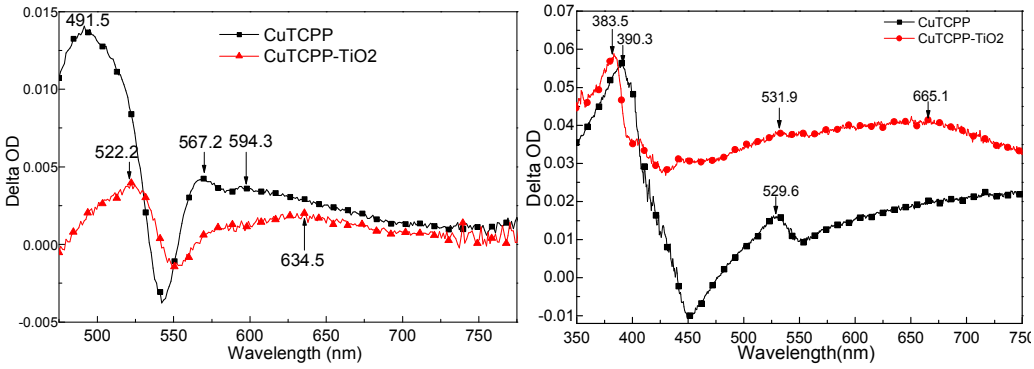

A B

Figure 3 Transient absorption spectra of CuTCPP and CuTCPP-TiO_2 : (A)collected 2ps delay after exciting at 400mm laser in the spectral range 475-775 nm with Femtosecond pulses. (B) collected 1ns delay after exciting at 355mm laser in the spectral range 350-750 nm with nanosecond pulses.

Fig. 3 presents the Femtosecond(A) and nanosecond(B) TA spectra of CuTCPP and CuTCPP-TiO_2 dispersed in MeCN. We used MeCN as the solvent to disperse the CuTCPP and CuTCPP-TiO_2 because Acetonitrile (MeCN) is a slow holes scavenger of TiO_2 and the reaction between MeCN and holes is not detected on the Femtosecond time scale. The TA spectra were obtained by subtracting the absorption spectrum in the original state from the spectrum measured at certain delay time. After Soret band wavelength photo excitation, three distinct bands could be clearly observed in CuTCPP in Femtosecond TA(Fig. 3A), one strong band sited at 491.5nm and other two broad bands with peaks sited at 567.2nm and 594.3nm respectively. While only two weak bands could be detected in CuTCPP-TiO_2 in Femtosecond TA(Fig. 3A), one band at 522.2nm and another broad band sited at 634.5nm, as for nanosecond TA(Fig. 3B), the 390.3nm TA band in CuTCPP was blue shift to 383.5nm in CuTCPP-TiO_2. The negative bands at 450nm (assigned as fluorescence of the CuTCPP) in CuTCPP disappeared in CuTCPP-TiO_2 and additionally there seems a very broad band across the whole region from 450 to 750. This broad absorption band comes from the electron-holes separation states of TiO_2 nanoparticles. That is, the absorptions of holes and electrons overlapped with each other in the broad absorption range. According to the literature, the band centered at 520nm and 1200nm are assigned as trapped holes on TiO_2 and the band centered at 770nm is assigned as trapped electrons [32]. A precise assignment

of the absorptions of electrons and holes is rather difficult because their absorption spectra are very broad and the bands overlap each other. In Fig.3B, the very broad absorption band range from 450nm to 750nm suggest that some holes and electrons are photogenerated and are trapped separately.

Since the transient absorption patterns shows very different after CuTCPP anchored to TiO_2 nanoparticles as shown in figure 3, undoubtedly the kinetic behaviors shows different way also as discussed below.

Figure 4 shows the Femtosecond transient decay profile of CuTCPP measured at three different probe wavelengths when pumping the Soret band. The transient at 491.5 nm rises to the maximum at ~1.21 ps and then decays on the picosecond time scale. The transients at 567.2nm and 594.3 nm rise to the maximum at ~3.30 ps simultaneously and then decay individually. The maximum of transient at 567.2nm and 594.3 nm are lag 2.09ps behind that of transient at 491.5 nm. The TA at 491.5nm shown in Figure 4 was well fit with three picosecond exponential components (lifetimes 0.90, 19 and 120 ps). As to the relaxation dynamics of the transient at 567.2nm and 594.3 nm, note that they appears as a rise after the inflexion (1.21ps) by the decay of the transient at 491.5nm, The fit parameters are given in Table I, the nanosecond TA fit parameters are also included. Three different femtosecond range lifetime and one nanosecond lifetime components contribute to the signal of the relaxation dynamics of CuTCPP. Note that the femtosecond lifetime appears as a rise at 567.2nm and 594.3 nm while appears as decline at 491.5 nm, which consistent with the inter conversion process of S_2 →S1. The broad picture confirms general features of the ultrafast dynamics and be represent schematically in figure 5, this is similar to previous studies in other porphrines:[21, 33] the lifetime of $\boldsymbol{\tau_3}$ is in consistency with the characterization of TCSPC in figure 2, so we assigned the $\boldsymbol{\tau_3}$ as the S_2 →S1fluorescence process. The overview of the dynamic process describes as: For excitation around 400 nm, relaxation of S_2 by internal conversion (IC) and the rise of S_1 occur in about 0.9 ps, followed by a slower vibrational relaxation by energy loss to the solvent on a time scale on the order of 6-19 ps and S_2 →S0 fluorescent process on a time scale of 100-120 ps, and finally S_1 decay (intersystem crossing + fluorescence), time constant 16-18 ns.

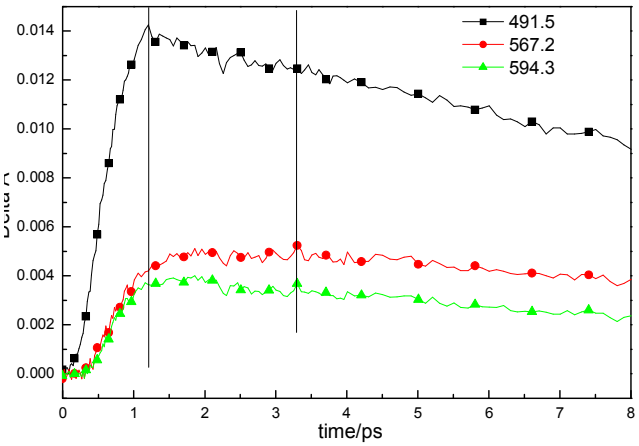

Figure 4 Transient absorption decay profile of CuTCPP dispersed in MeCN at three different probe wavelengths

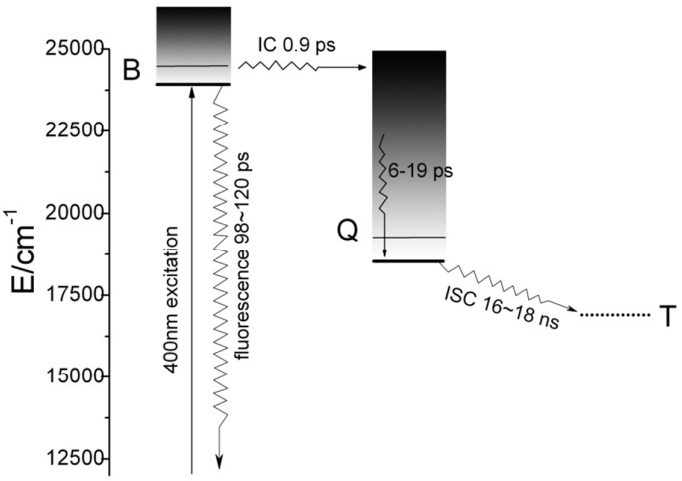

Figure 5 Schematic diagram of the energy relaxation dynamics of CuTCPP. Solid horizontal lines are located at the energies of bands in the absorption spectrum. Dashed lines indicate approximate energies for T1. See text for details of the dynamics.

TABLE 1: Multiexponential Fittings of the Observed Kinetic Profiles of CuTCPP **Shown in Figures 3 and 4: Time Constants (τ, ps), Amplitudes (A), and Wavelengths (λprobe, nm)***a*

λprobe	Lifetimes			relative amplitudes[a]		
	τ_1	τ_2	τ_3	A_1	A_2	A_3
491.5	0.90	19	120	0.0040	0.0117	0.0026
567.2	0.55	7	120	-0.0091	0.0029	0.0034
594.3	0.50	6	101	-0.0088	0.0029	0.0020
390.3	17173			5.52E30		
529.6	16827			1.04E31		

a A negative amplitude indicates that the respective component is a rise instead of a decay.

TABLE II: Multiexponential Fittings of the Observed TA spectra of CuTCPP-TiO_2 **Shown in Figures 3: Time Constants (τ, ps), Amplitudes (A), and Wavelengths (λprobe, nm)***a*

λprobe	Lifetimes			relative amplitudes[a]		
	τ_1	τ_2	τ_3	A_1	A_2	A_3
491.5	0.43	24	319	0.0015	0.0012	0.0015
521.0	0.43	33	382	-0.0092	0.0018	0.0026
632.2	0.33	26	398	-0.0116	0.0009	0.0014
383.5.3	36578			9.98E13		
600	46883			6.59E10		

a A negative amplitude indicates that the respective component is a rise instead of a decay.

For the case of CuTCPP-TiO_2, the relaxation of S_2 process is very similar to CuTCPP, however the every lifetime of components step is different, which have been show in Table II. Especially, the S2 and S1 state of CuTCPP-TiO_2 have been quenched as shown in figure 1, so the TA of femtosecond spectra is very weak, and made the fitted lifetime ambiguous, τ_3 is largely different from the TCSPC result. the nanosecond spectra however is stronger than CuTCPP, as shown in

figure 3 B. Although the S1 state is completely quenched as shown in figure 1, the electron-holes separation states of TiO_2 nanoparticles is appears in this absorption region. In general, the relaxation of S_2 by internal conversion (IC) and the rise of S_1 occur in about 0.5 ps, followed by a slower vibrational relaxation by energy loss to the solvent on a time scale on the order of 24-33 ps and S_2 →S0 fluorescent process on a time scale of 123 ps, and finally the electron-holes separation states decay, time constant 36-47 ns.

In general, there are two types of charge recombination channels[17]. The first is a fast (geminate) recombination process, which occurs between an oxidized dye and the injected electron that originates from the same dye. Matthew JG reported the very interesting sub-ns (0.5 ns to 100 ns) charge recombination channel between photo-injected electrons and porphyrin cations recently, The second process proceeds on a millisecond time scale and occurs between electrons and either oxidized dye molecules or the redox mediator. Our observation is in consistency to the fast recombination process and be assigned as the recombination between oxidized dye and the injected electron.

Phase composition

XRD was carried out to investigate the crystal identity of TiO_2 samples and the effect of CuTCPP on the crystal structure of TiO_2. Fig. 6 shows the typical XRD pattern of CuTCPP-TiO_2 and P25 nanoparticles. The P25 powder contains 20% rutile and 80% anatase. The diffraction peaks at 2θ = 25.3, 37.8, 48.0, 53.1, 55.4, 62.7, 68.8, corresponds to the (101), (004), (200), (105), (211), (204),and (116) planes of anatase TiO_2, respectively. The peak of which were strong and in good agreement with the standard XRD patterns of anatase (JCPDS No. 84−1286). While the peak at 27.4°,36.1°and 41.5° are also present, indicating there coexists the rutile phase (JCPDS No. 88-1175). Based on the Scherrer formula, the crystallite sizes of P25 is about 20nm and the CuTCPP-TiO_2 is 20nm. These results indicate that the CuTCPP sensitized on the surface of TiO_2 hardly has any effect on the crystal structure of TiO_2 powders.

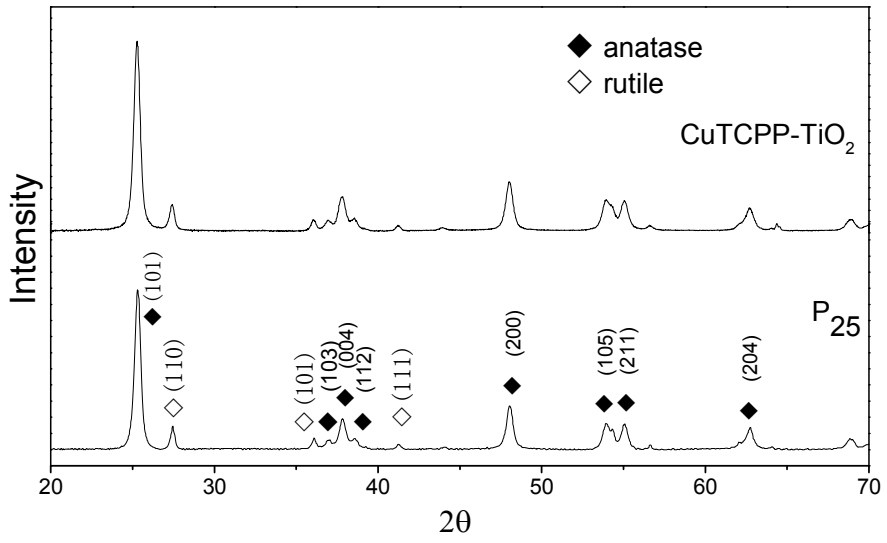

Figure 6 XRD patterns of CuTCPP-TiO_2 and P25. ◆stands for anatase, ◇for rutile.

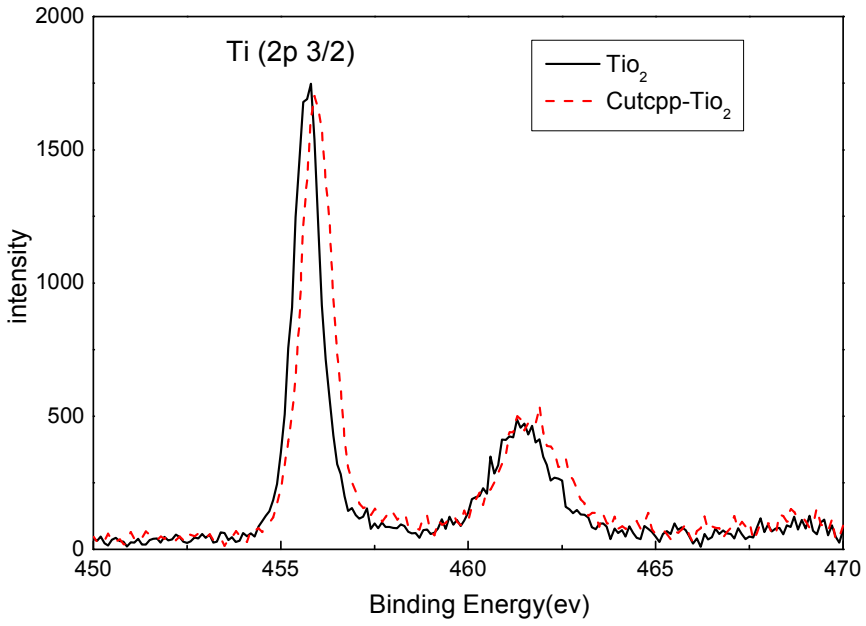

Figure 7 XPS of the Ti 2p regions

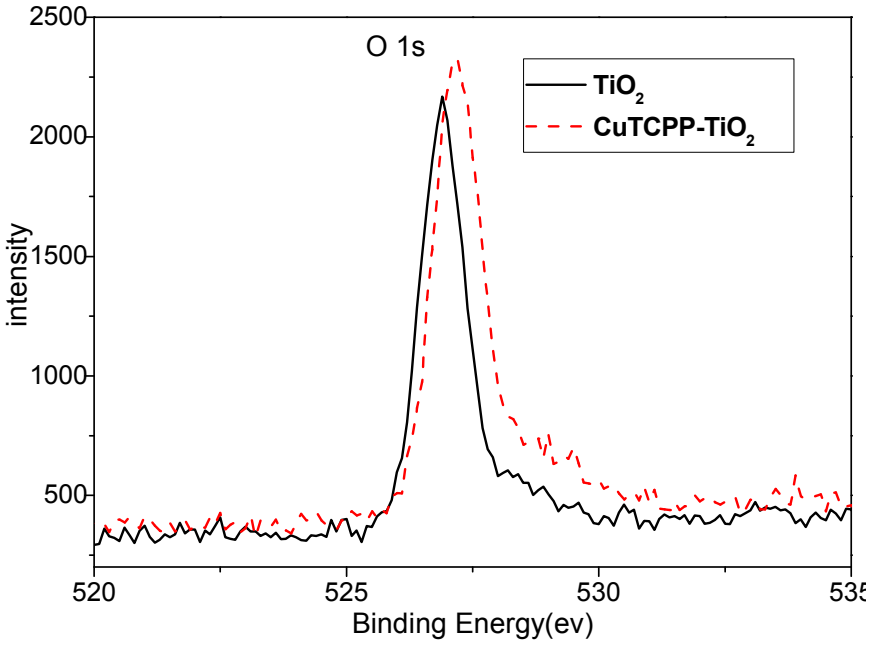

Figure 8 XPS of the O 1s regions

XPS was used to distinguish the surface change of pure TiO_2 and CuTCPP-TiO_2. Figs. 7 and 8 show Ti 2p and O 1s XPS spectra of pure TiO_2 and CuTCPP sensitized TiO_2 respectively. The Ti ($2p_{3/2}$) binding energy values of TiO_2 and CuTCPP-TiO_2 are 455.8 and 455.9 respectively. The peak of CuTCPP-TiO_2 is higher 0.1 eV than that of pure TiO_2. This data suggest that H atom as

the donor coordinates with oxygen atom in Ti-O-H in TiO_2 and that the oxygen atom accepts electrons. When the CuTCPP sensitized to TiO_2 the Carbonyl group substitute the H as Ti-O-C=O, contrary to the H group, Carbonyl is a electron-accepting groups, it withdraw electrons from O atoms and then raised the valence of Ti atom, decreased the density of the layer electron cloud, leading to the increase in the binding energies of the Ti ($2p_{3/2}$). The attraction of electron from O atom also leading to the decrease of the electron cloud density of O atom, raising the valence of O atom and consequently increase in the binding energies of the O 1s, which can be demonstrated in O 1s XPS spectra shown in figure 7. The adsorption mechanism of CuTCPP on the TiO_2 surface can be attributed to the weak chemisorptions.

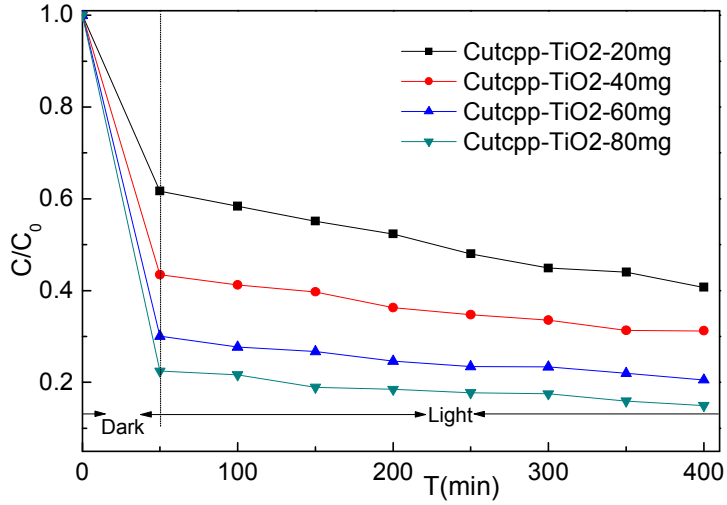

Figure 9 Evolution of MB concentration as a function of time: 50 min in the dark followed of 400 min under visible light irradiation.

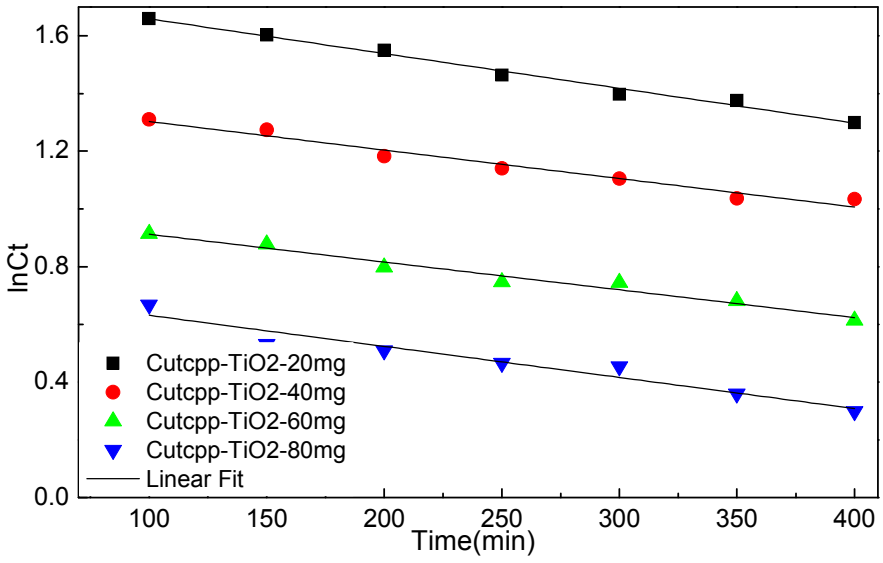

Figure 10 First order linear fitting of disappearance of MB by photocatalysis under visible light irradiation

Photocatalytic Activity of CuTCPP-TiO_2.

It is well known that the photocatalysis activity depends on the crystallinity, phase, and the surface area of the materials. In this work, the visible light induced photocatalytic activities of the as-synthesized CuTCPP sensitized TiO_2 were evaluated by photocatalytic degradation of MB under 250 W Iodine-Tungsten lamp illuminations with 420 nm cutoff filter. Our previous research shows that the adsorption process takes very quickly, completed in the first 50 minutes. Based on this date of absorbance experiments in the dark, all degradation reactions were allowed to stand in the dark for a period of 50 min to establish adsorption equilibrium, and then performs the visible light irradiation. As shown in Figure 9, The CuTCPP-TiO_2 can efficiently photo degrade MB under visible light irradiation. When the initial concentration 9 mg/L of MB was used, adding different amounts of CuTCPP-TiO_2 (20, 40, 60 and 80 mg) showed 59.28%, 68.76%, 79.47% and 85.02% decolorization rates (1-ct/c0), respectively, under Iodine-Tungsten lamp illumination after 400 min. Accordingly dark adsorption contributed 38.30%,56.52%, 69.91% and 77.53% to the reduction of MB concentration, respectively, indicating the significant photodegrade capacity of the CuTCPP-TiO_2 in the whole process. The high efficiency performance could be ascribed to its unique cooperative effects of strong adsorption ability and low band gap energy.

During the irradiation period, MB-photo degradation data were analyzed using the Langmuir–Hinshelwood kinetic model[34]: with the rate $-\frac{dC}{dt}$ being proportional to the coverage θ which becomes proportional to C at low concentrations: $-\frac{dC}{dt} = k\theta = \frac{kKC}{1+KC} \approx kKC = k_{app}C$

In all cases, a satisfactory linearity was obtained by applying Langmuir–Hinshelwood kinetic model (Fig. 10). Values of the apparent first-order constant, k_{app}, keeps constantly for different amount of CuTCPP-TiO_2, indicating it have no relation with the adding dose of catalysts.

4 Discussion

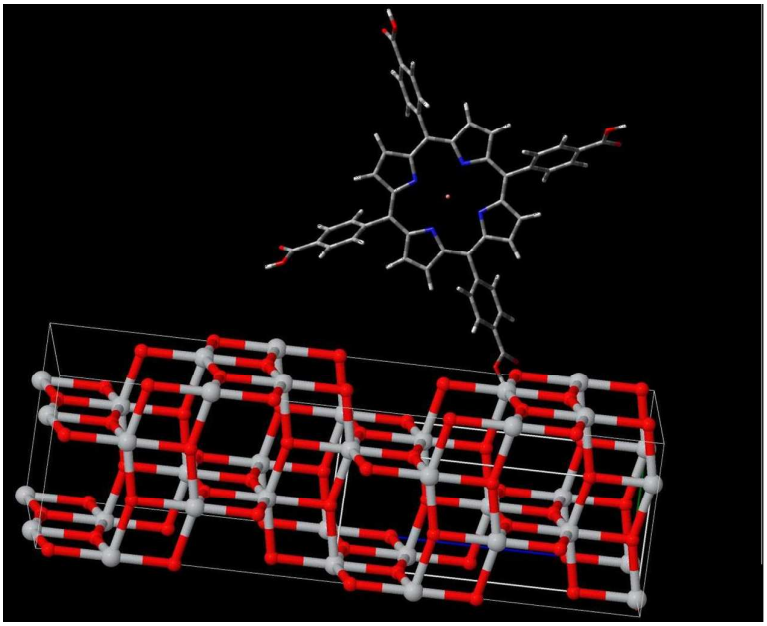

Figure 11 Scheme showing The Molecular structure for CuTCPP anchoring to the (101) surface of anatase

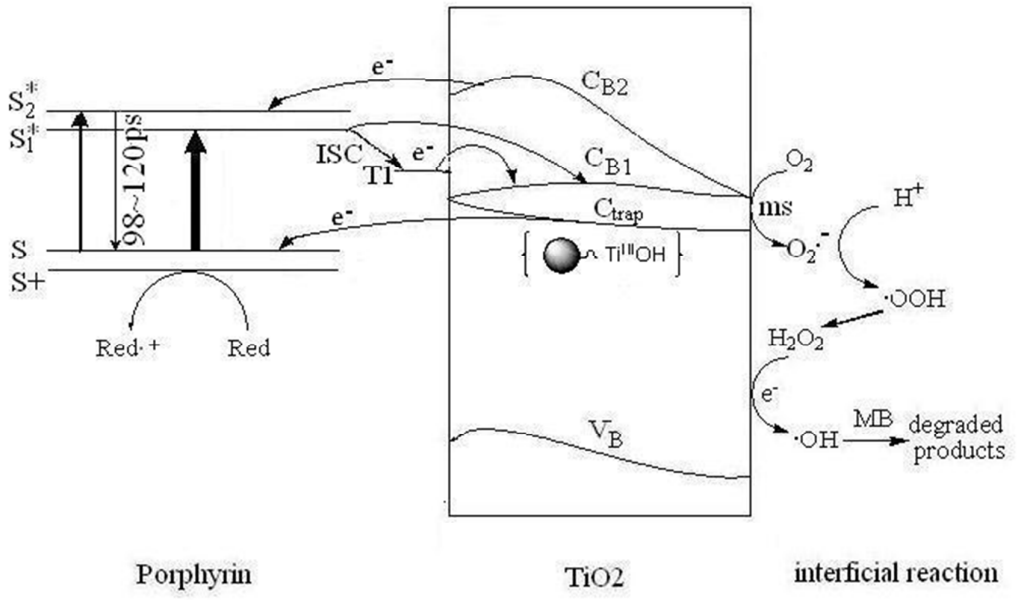

Figure 12 Schematic presentations of energy levels, basic photoinduced electron decay process, and photoinduced MB degradation mechanism

The first conclusion that we can draw from our data is that the CuTCPP is chemical linked to the anatase surface. Obviously, the only physical absorption between the sensitizer and anatase could not appreciably affect the electron states in each material. evidences of a chemical Ti-O-C=O link are provided by the fact that the blue-shift of the fluorescence spectra of CuTCPP-TiO_2 and the obvious binding energies changes in XPS spectra, as shown in Figures 1,2,3,7,8. The (101) anatase surface is the mostly exposed area for anatase nanocrystals[35], which we are using for the dye sensitizing in photodegradation. It is clear from Figure 11 that the electron hopping along the Ti-O-C=O chain is the main mechanism of the charge transport between the dye and the surface (101) of anatase. The C-O bond connects the sensitizer molecule to anatase, whereas the oxygen atom belongs to both materials.

The fluorescence spectra of CuTCPP and CuTCPP-TiO_2 demonstrated that, the emission from the S1 state to S0 state in the Franck-Condon active mode in CuTCPP is greatly quenched by the linking of TiO_2, and the emission from the S2 state is expected to lie at 487.7nm, however occurred at 469.0nm after link to TiO_2. These indicate that the coupling of $\boldsymbol{\pi}$ orbitals of the porphyrin with the Ti(3d) orbital opens the relaxation way of the electron transportation to C_{B1} state of TiO_2, and therefore, quenched the fluorescence intensity in S1-S0 process as observed in figure 1. Then to what physical processes in the excited states do the observed lifetimes correspond? The lifetime fitted in figure 2 could be definitely assigned as the lifetime of S2→S0 fluorescence process, then what is the lifetime fitted in nanosecond transient absorption decay profile in Table II? 680nm TA absorption is assigned as the shallow trapped conduction-band electron, so here we can assign the TA fitted lifetime as the recombination lifetime of trapped electron (See eq 6). And we find that the lifetime hasn't been changed after the TiO_2 sensitized with CuTCPP. The lifetime of this electron trapped state is vital for photocatalysis quantum efficiencies.

On the basis of the references[24] and our dynamic measurements we proposed the following

mechanism for heterogeneous photocatalysis on CuTCPP-TiO_2. Characteristic times for the various steps in the mechanism are given to the right of each step.

electron-holes separation

$$S + h\upsilon \longrightarrow S_1^* \qquad \text{(fs)} \quad \text{eq 3}$$

$$S_1^* \longrightarrow e^-_{CB1} + S^+ \qquad \text{(fs)} \quad \text{eq 4}$$

electron trapping

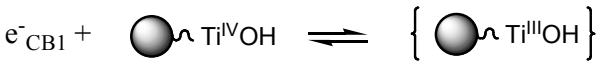

(100 ps) eq 5

electron-holes recombination

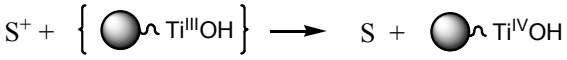

(47 ns) eq 6

interfacial electron transfer

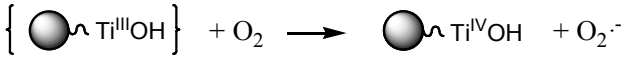

(ms) eq 7

$$S^+ + \text{Red} \longrightarrow S + \text{Red}^{\cdot +} \qquad \text{(100ns)} \quad \text{eq 8}$$

where 

represents the primary hydrated surface functionality of TiO_2, e^-_{CB1} is a conduction-band electron, Red is an electron donor (i.e., reductant), 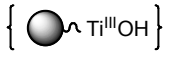

is the surface-trapped CB1 electron.

The pathways and time scales for relaxation of excited state of CuTCPP-TiO_2 as discussed in the preceding paragraphs are represented schematically in Figure 12. When the visible light irradiates on the surface of CuTCPP-TiO_2 nanoparticles, the electrons in CuTCPP can be excited from the S0 level to the "S1" or "S2" of the porphyrin ring (π*). Then the electron in S2 state comes back to the original S0 level accompanied by the photon emission whereas the electron in S1 state have two pathways: leaves for the P25 C_{B1} via the Ti-O bond and intersystem crossing to T1. The dominant channel for Q*x* relaxation is intersystem crossing to T1, and the lifetime of the T1 state is reported to be milliseconds in degassed solvents[36]. Subsequently, the electron in C_{B1} was trapped in 100ps by the reaction as shown in eq 5. Then the trapped electron 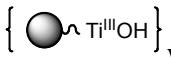

will, either recombine with holes depicted as eq 6, or interfacial transfer to encounter with O_2 adsorbed on the surface to reduce to $O_2^{\bullet -}$, which can further transform into H_2O_2 and •OH, resulting in the oxidation of MB finally. Meanwhile, the reactive holes S^+ can oxidize MB to its radical cation either directly or through a primarily formed •OH produced by the oxidation of ubiquitous water.

According to the mechanism illustrated in Figure 12 and eq 6 and eq 7, the overall quantum efficiency for interfacial charge transfer is determined by two critical processes. They are the competition between electron-holes recombination and trapping (picoseconds to nanoseconds) followed by the competition between trapped electron recombination and interfacial charge transfer (microseconds to milliseconds). The prolonged lifetime in trapped electron-holes recombination favors the interfacial charge transfer and enhances the degradation efficiency.

5 Conclusions

CuTCPP were chemically sensitized on the surface of TiO_2 to act as visible light antenna and to modify the photoresponse properties of TiO_2 particles. The TCSPC technique combined with their fluorescence spectra revealed that the S2-S0 fluorescence of CuTCPP is decreased in intensity by TiO_2 and blue shifted by 18.7nm in wavelength, with the lifetime prolonged. Ti 2p and O 1s XPS spectra of pure TiO_2 and CuTCPP-TiO_2 provide a direct demonstration for the formation of Ti-O-C=O bond.

The CuTCPP-TiO_2 exhibits better photoactivity under visible light irradiation than that of pure TiO_2. The photocatalytic degradation kinetics of MB fitted well with Langmuir–Hinshelwood mode. This efficiency in the MB-photocatalytic activity of CuTCPP-TiO_2 could be due to a combined effect of the potential photosensitivity of the CuTCPP-TiO_2 band gap, the increase in MB adsorption capacity and the prolonged lifetime for electron transfer from photo-excited porphyrin to the surface of TiO_2.

The development of the porphyrin-based photocatalyst provides an alternative approach in harnessing solar visible light. Further investigations about the adsorption and photocatalysis behaviors should be made to obtain deeper insight into the cooperative action mechanism between them.

Acknowledgements

This work was supported by grants from Alexander von Humboldt Foundation, National Natural Science Foundation of China (No. 21271155 and 21273202), Natural Science Foundation of Zhejiang Province (No. LY13B030009) and Zhejiang SCI-TECH University for 521 Distinguished Scholars scheme.

References

1. J. E. Johnston and J. M. Gibson, *Environmental Science & Technology*, 2013, **47**, 5595-5602.
2. X. M. Wang, L. J. Xing, T. L. Qiu and M. L. Han, *Environmental Science and Pollution Research*, 2013, **20**, 2236-2243.
3. G. M. Ratnamala, K. V. Shetty and G. Srinikethan, *Water Air and Soil Pollution*, 2012, **223**, 6187-6199.
4. P. Punamiya, D. Sarkar, S. Rakshit and R. Datta, *J. Environ. Qual.*, 2013, **42**, 1449-1459.
5. O. F. Olorundare, R. W. M. Krause, J. O. Okonkwo and B. B. Mamba, *Phys. Chem. Earth*, 2012, **50-52**, 104-110.
6. R. M. Hlihor and M. Gavrilescu, *Environ. Eng. Manag. J.*, 2009, **8**, 353-372.
7. U. C. Panda, P. Rath, S. Bramha and K. C. Sahu, *Journal of Coastal Research*, 2010, **26**, 860-868.
8. L. Vezzaro, E. Eriksson, A. Ledin and P. S. Mikkelsen, *Water Research*, 2012, **46**, 6891-6903.
9. S. Sarkar, A. Makhal, T. Bora, K. Lakhsman, A. Singha, J. Dutta and S. K. Pal, *ACS Appl. Mater. Interfaces*, 2012, **4**, 7026-7034.
10. S. Ardo, D. Achey, A. J. Morris, M. Abrahamsson and G. J. Meyer, *Journal of the American Chemical Society*, 2011, **133**, 16572-16580.
11. D. Li, W. J. Dong, S. M. Sun, Z. Shi and S. H. Feng, *Journal of Physical Chemistry C*, 2008, **112**, 14878-14882.

12. J. Ananpattarachai, P. Kajitvichyanukul and S. Seraphin, *Journal of Hazardous Materials*, 2009, **168**, 253-261.
13. J. H. Cai, J. W. Huang, H. C. Yu and L. N. Ji, *International Journal of Photoenergy*, 2012.
14. M. K. Panda, K. Ladomenou and A. G. Coutsolelos, *Coordination Chemistry Reviews*, 2012, **256**, 2601-2627.
15. M. Pelaez, N. T. Nolan, S. C. Pillai, M. K. Seery, P. Falaras, A. G. Kontos, P. S. M. Dunlop, J. W. J. Hamilton, J. A. Byrne, K. O'Shea, M. H. Entezari and D. D. Dionysiou, *Applied Catalysis B-Environmental*, 2012, **125**, 331-349.
16. C. Wang, X. X. Ma, J. Li, L. Xu and F. X. Zhang, *Journal of Molecular Catalysis a-Chemical*, 2012, **363**, 108-114.
17. M. J. Griffith, K. Sunahara, P. Wagner, K. Wagner, G. G. Wallace, D. L. Officer, A. Furube, R. Katoh, S. Mori and A. J. Mozer, *Chemical Communications*, 2012, **48**, 4145-4162.
18. W. J. Sun, J. Li, G. P. Yao, M. Jiang and F. X. Zhang, *Catal. Commun.*, 2011, **16**, 90-93.
19. W. Kim, J. Park, H. J. Jo, H. J. Kim and W. Choi, *Journal of Physical Chemistry C*, 2008, **112**, 491-499.
20. G. Mele, R. Del Sole, G. Vasapollo, G. Marci, E. Garcia-Lopez, L. Palmisano, J. M. Coronado, M. D. Hernandez-Alonso, C. Malitesta and M. R. Guascito, *Journal of Physical Chemistry B*, 2005, **109**, 12347-12352.
21. A. Marcelli, I. J. Badovinac, N. Orlic, P. R. Salvi and C. Gellini, *Photochemical & Photobiological Sciences*, 2013, **12**, 348-355.
22. A. Marcelli, P. Foggi, L. Moroni, C. Gellini and P. R. Salvi, *Journal of Physical Chemistry A*, 2008, **112**, 1864-1872.
23. V. N. Knyukshto, E. I. Sagun, A. M. Shulga, S. M. Bachilo and E. I. Zenkevich, *Chem. Phys. Rep.*, 1999, **18**, 855-872.
24. M. R. Hoffmann, S. T. Martin, W. Y. Choi and D. W. Bahnemann, *Chemical Reviews*, 1995, **95**, 69-96.
25. J. R. McCarthy and R. Weissleder, *ChemMedChem*, 2007, **2**, 360-365.
26. K. Rurack, *Spectroc. Acta Pt. A-Molec. Biomolec. Spectr.*, 2001, **57**, 2161-2195.
27. D. F. Marsh and L. M. Mink, *Journal of Chemical Education*, 1996, **73**, 1188-1190.
28. J. M. Wan, H. G. Wang, Z. Z. Wu, Y. C. Shun, X. M. Zheng and D. L. Phillips, *Physical Chemistry Chemical Physics*, 2011, **13**, 10183-10190.
29. H. G. Wang, J. Xu, J. M. Wan, Y. Y. Zhao and X. M. Zheng, *Journal of Physical Chemistry B*, 2010, **114**, 3623-3632.
30. L. H. Yu, J. Y. Xi, M. D. Li, H. T. Chan, T. Su, D. L. Phillips and W. K. Chan, *Physical Chemistry Chemical Physics*, 2012, **14**, 3589-3595.
31. A. Kathiravan, P. S. Kumar, R. Renganathan and S. Anandan, *Colloids and Surfaces a-Physicochemical and Engineering Aspects*, 2009, **333**, 175-181.
32. T. Yoshihara, R. Katoh, A. Furube, Y. Tamaki, M. Murai, K. Hara, S. Murata, H. Arakawa and M. Tachiya, *Journal of Physical Chemistry B*, 2004, **108**, 3817-3823.
33. H. Z. Yu, J. S. Baskin and A. H. Zewail, *Journal of Physical Chemistry A*, 2002, **106**, 9845-9854.
34. A. Houas, H. Lachheb, M. Ksibi, E. Elaloui, C. Guillard and J. M. Herrmann, *Applied Catalysis B-Environmental*, 2001, **31**, 145-157.
35. G. Spoto, C. Morterra, L. Marchese, L. Orio and A. Zecchina, *Vacuum*, 1990, **41**, 37-39.
36. L. Pekkarinen and H. Linschitz, *Journal of the American Chemical Society*, 1960, **82**,

2407-2411.